A numerical-experimental coupled method for the identification of model parameters from μ-SPIF test using a finite element updating method

Karim Belouettar, Sébastien Thibaud, Mohand Ould Ouali, Mohamed Karim Harouche

A numerical-experimental coupled method for the identification of model parameters from µ-SPIF test using a finite element updating method

Belouettar Karim*[1] . Thibaud Sébastien [2] . Ould Ouali Mohand [3] . Harouche Mohamed Karim [4]

[1] Advanced Manufacturing and Control Techniques Laboratory, Ecole Militaire Polytechnique (EMP), Algiers 16111, Algeria
karim.belouettar@emp.mdn.dz

[2] FEMTO-ST Institute, Univ. Bourgogne Franche-Comté, CNRS/UFC//ENSMM/UTBM, 25000 Besançon, France

[3] Laboratory of Elaboration and Characterization of Materials and Modeling (LEC2M), University of Tizi-Ouzou 15100, Algeria

[4] Engineering Materials Laboratory, Ecole Militaire Polytechnique (EMP), Algiers 16111, Algeria

Abstract

Single Point Incremental forming (SPIF) is a technology that allows obtaining complex parts using a hemispherical end tool by applying a local deformation process in sheet metal. This dieless process presents the advantage of high formability limits and low cost. The increasing need for micro components, namely in the medical industry (implants and medical tools and accessories), has contributed to the development of the micro single-point incremental forming (µ-SPIF) technique. However, this technique requires meeting certain challenges related to tool wear, resistance and precision of the manufactured parts, and increased formability. So, understanding the deformation and failure mechanisms in µ-SPIF is important to achieve improved formability. This paper aims to improve the predictions of the shear-modified GTN damage model by proposing an identification procedure for its numerous material parameters based on an inverse method coupling the numerical predictions with experimental results. The extended GTN model is first implemented into the finite element code Abaqus. The numerical approach is assessed through numerical simulations under shear and uniaxial tension loading. Then, a complete methodology is proposed to identify the set of material parameters using tensile and micro single-point incremental forming (µ-SPIF) experimental results. The identification approach is based on the comparison of the numerical and experimental forces used to carry out the micro-incremental forming test with a pyramidal shape tool. To show the pertinence of the identification procedure, the numerical predictions of the modified GTN model with these material parameters are compared to the experimental results of µ-SPIF tests with different tool paths and geometrical forms. Finally, It is shown that the shear modification of the GTN model can predict the failure of sheets during metal forming.

Keywords: Micro-single point incremental forming. GTN model. Shear damage. Ductile damage model. Finite element method. Identification. Inverse method.

1. Introduction

Incremental sheet forming is one of the essential techniques used in industry for the manufacturing of thin sheet metal components for a large number of application domains [1]. The desired geometry is obtained by using a specific forming tool path controlled by a CNC machine. The main advantage of this process is its very low cost. However, there is some need to master the influence of some process parameters to avoid damage and rupture of the sheet during forming. The conducted studies focus on the prediction of damage evolution until failure in a square sheet copper alloy.

It's well known that the failure process in ductile metallic materials occurs under three stages, i.e. micro-void nucleation, growth, and coalescence. Several coupled and uncoupled models have been proposed to study the damage by the growth of cavities (voids) from the pioneering works of McClintock [2] and Rice and Tracey [3]. Gurson [4] proposed a coupled constitutive model based on a micromechanical approach. Afterward, Tvergaard and Needleman [5–7] modified the original Gurson model by adding three additional parameters to describe the ductile fracture of material due to nucleation, growth, and coalescence of spherical cavities. This formulation, the so-called Gurson-Tvergaard-Needleman (GTN) model, is widely used to study the ductile fracture of metals [8–14]. More recently, an important limitation of the original GTN model is established. It is related to the fact that shear states are not taken into account in the formulation. Therefore, the model cannot predict correctly the localization of shear bands and failure under relatively low or even negative stress triaxiality [15, 16]. To remedy this situation, Xue [17], Nahshon, and Hutchinson [18] put forward a shear-modified GTN model to take into account the accumulation of effective damage caused by void distortion due to shear strain. The accuracy of the modified GTN model in the prediction of ductile failure is the subject of several studies [19–22].

For the prediction of ductile fracture during single point incremental forming (SPIF), Gatea et al. [23] conduct a comparison between the original GTN model and the GTN modified by Nahshon and Hutchinson [18]. Belouettar et al. [24] studied the influence of some process parameters using response surface methodology and the GTN damage model to analyze the damage evolution during material deformation. An implementation of the shear mechanism in the GTN damage model is validated by Ying et al. [25] for tensile and shear tests for use in the Small Punch Test (SPT) modeling. Achouri et al. investigate the damage behavior for different stress states by the modified GTN model [26, 27]. It demonstrated that the model can predict ductile fracture due to shear in the punching process application.

It is well known that fine prediction of failure by the GTN model depends on the accurate determination of its various material parameters set. Several methods are developed for the identification of the GTN's model parameters. A method based on artificial neural networks (ANN) combined with experimental tests and numerical simulations is used in many studies to identify these parameters in different applications. Aguir et al. [28] and Marouani et al. [29] considered the sheet metal blanking technique. Abbassi et al. [30] calibrated the parameters by using the results of the notched tensile test, bulge test, and Erichsen test. Sun et al. [31] identified the material parameters of a shear-modified GTN damage model by the small punch test. Achouri et al. [27] propose an identification strategy for the modified GTN model using experiments on specimens with different shapes under low and high-stress triaxiality conditions. Another important approach widely used to calibrate the model's parameters is the inverse method coupled with a non-linear optimization procedure. The principle of this method is to quantitatively describe responses and minimize the difference between experimental tests and the corresponding numerical simulation results by using an advanced optimization technique. The identification of the model parameters with the inverse methods is carried out using classical tensile tests, compression, bending, and shear tests [32–35]. It is noticed that the generated strain level by these tests is lower and limited, therefore, the necking phenomenon is not represented, which makes the identification difficult in the case of complex and large deformation produced by damage level. Hence, the identification by classical tests is not sufficient to correctly predict material behavior during metal forming operations.

Several authors proposed an approach that combines classical and advanced tests (deep drawing, small punch…) with measurement data to determine constitutive parameters. Ghouati and Gelin used this approach to directly identify the material parameters from the metal-forming process [36]. The initial parameters set of the elastoplastic law are determined from the tensile test results of an aluminum alloy. Then the deep drawing test is used as a second step of identification. Ben Hamida et al. [37] and Hapsari et al. [38] developed a procedure for ductile damage parameters identification by an inverse finite element method applied for tensile and micro incremental forming tests named InDef tests.

This paper is dedicated to the identification of the optimum material parameters of an extended anisotropic Gurson model taking into account shear mechanisms to predict ductile fracture during the micro Single Point Incremental Forming process (μ-SPIF) of a copper alloy sheet. In this context, the forming force measurement is adopted to characterize the material behavior of thin sheet metals from micro-single point incremental forming tests. The modified GTN damage model is implemented through the user-defined material subroutine

(VUMAT) into Abaqus/explicit. The implementation is validated by numerical tests (uniaxial tensile and simple shear) on a single element. The identification of the GTN damage model parameters is carried out based on tensile and μ-SPIF test results. For this purpose, the finite element updating method (FEUM) is used. Finally, the reliability of the identified parameters is verified by μ-SPIF tests on different tool paths and geometrical forms.

2. Modified GTN model

2.1 Yield surface definition

A micromechanical GTN model is chosen for the prediction of the damage and ductile fracture of materials which is based on the initial Gurson model [4]. In its basic form, Gurson's model represents only porosity growth to quantify material degradation during loading. New parameters of damage were added to the expression of the yield surface and the introduction of nucleation and coalescence phenomena were taken into account. With these modifications, the extended version of the Gurson model defined as the GTN's model is expressed by:

$$\phi = \left(\frac{\sigma_{eqv}}{\sigma_y} \right)^2 + 2q_1 f^* \cosh\left(-3q_2 \frac{\sigma_m}{2\sigma_y} \right) - \left(1 + \left(q_1 f^* \right)^2 \right) = 0 \tag{1}$$

Where σ_{eqv} is the von Mises equivalent stress, initially equal to σ_y (initial yield stress), σ_m is the hydrostatic stress and (q_1, q_2) are the Tvergaard's coefficients.

The function $f^*(f)$ defines the void volume fraction of the GTN model expressed by

$$f^* = \begin{cases} f & f < f_c \\ f_c + \dfrac{\bar{f}_F - f_c}{f_F - f_c}(f - f_c) & \text{if} \quad f_c < f < f_F \\ \bar{f}_F & f \geq f_F \end{cases} \tag{2}$$

where f is the void volume fraction, initially equals to f_0, f_c is the critical void volume fraction, f_F is the void volume fraction at fracture and $\bar{f}_F = 1/q_1$.

The evolution of the void volume fraction is given by

$$\dot{f} = \dot{f}_{growth} + \dot{f}_{nucleation} \tag{3}$$

With

$$\dot{f}_{growth} = (1 - f)\, tr\left(\dot{\varepsilon}^P\right) \tag{4}$$

and

$$\dot{f}_{nucleation} = A\dot{\bar{\varepsilon}}^P = \frac{f_N}{S_N\sqrt{\pi}} exp\left[-\frac{1}{2}\left(\frac{\bar{\varepsilon}^P - \varepsilon_N}{S_N} \right)^2 \right] \dot{\bar{\varepsilon}}^P \tag{5}$$

where f_N is the void volume fraction due to the nucleation of new cavities, ε_N the plastic strain at the start of nucleation, s_N and the standard deviation of the nucleation strain. $\bar{\varepsilon}^p$ and $\dot{\bar{\varepsilon}}^p$ represent respectively the equivalent plastic strain and the equivalent plastic strain rate in the material matrix.

2.2 Shear effects

In the original GTN model, the measurement of the increment of void volume fraction is based on the nucleation and growth of voids. In this study, the Nahshon-Hutchinson type shear mechanism is incorporated in the GTN model to take into account the effect of shear in the increment of void volume fraction. Therefore, to extend the applicability, K. Nahshon et al. introduced a modification term into the GTN model [18]:

$$\dot{f}_{shear} = k_w \frac{f\, w_0(\sigma)}{q} s : \dot{\varepsilon}^p \tag{6}$$

where $w_0(\sigma)$ is a function of the stress state, characterized by the normalized third invariant of the deviatoric stress tensor ($\xi = 27 J_3 / 2q^3$), $s = \sigma + pI$. I is the second order unit tensor. The k_w parameter is the magnitude of the shear growth rate. $w_0(\sigma)$ is given by

$$w_0(\sigma) = w(\xi) = 1 - (\xi)^2 = 1 - 27 J_3 / 2q^3 \tag{7}$$

where $J_3 = \det(s)$ is the third invariant of the deviatoric stress tensor.

Finally, after the addition of the new contribution for shear loads, the evolution of the total void volume fraction becomes:

$$\dot{f} = (1 - f)\, tr(\dot{\varepsilon}^p) + A\dot{\bar{\varepsilon}}^p + k_w \frac{f\, w_0(\sigma)}{q} s : \dot{\varepsilon}^p \tag{8}$$

The corresponding implementation method of the modified Gurson model in shear loading is developed in the ABAQUS/Explicit finite element code, using a user material constitutive subroutine (VUMAT). The implementation of the constitutive law is carried out using the algorithm proposed by Aravas for pressure-dependent plasticity models, which is also based on elastic prediction and plastic correction [39–42].

2.3 Validation tests on single elements

In this section, the model implementation is verified using numerical simulation tests. A single 8-node brick element with one integration point (C3D8R) is selected to simulate uniaxial tension and simple shear tests. The initial size of each element edge is 1 mm. A value of 0.01 m/s of the loading velocity is taken for both tests to limit dynamic effects from the explicit algorithm. The boundary conditions are shown in Figure 1. To simulate the test cases,

the material parameters are chosen from Nahshon et al. [42] and Achouri et al. [26]. The results of the validation are shown in Figures 2 and 3 respectively.

- Material hardening low:

For the plastic flow definition, the von Mises yield criterion is used. Hardening evolution is based on an isotropic hardening law given by

$$\sigma = \sigma_y + K(\varepsilon^p)^n \tag{9}$$

where $\sigma_y = 200\ MPa$ is the initial yield stress, $K = 500\ MPa$ the material consistency, and $n = 0.1$ the hardening exponent.

- Damage parameters:

The constants $q_1 = q_2 = 1$, $f_0 = 0.005$, $\varepsilon_N = 0.3$, $S_N = 0.1$, $f_N = 0.04$ and k_w takes three values: 0, 1, and 3. f_0 is the initial void volume fraction in the material.

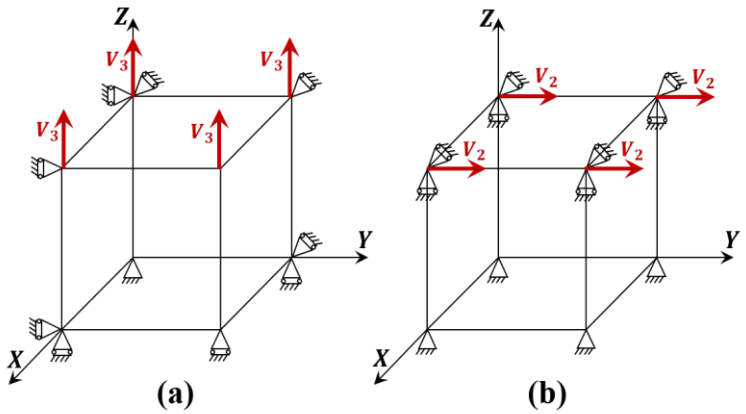

Fig. 1. Single element and boundary conditions for (a) uniaxial tension and (b) simple shear tests.

1- Uniaxial tension test

Effective stress and the void volume fraction evolutions as a function of equivalent plastic strain are illustrated in Figure 2. The obtained results of the modified model are perfectly superposed with the original GTN model for the axial stress (figure 2a) and the porosity (figure 2b). It can be observed that the results are independent of the k_w value in the tension condition.

2- Simple shear test

In the case of a simple shear test, i.e. $w(\sigma) = 1$, the results are expressed with the evolution of the effective stress and void volume fraction as a function of equivalent plastic strain for different k_w values (Figures 3a and 3b). The increase of k_w induces the decrease of the strain in the zone corresponding to damage localization. For the case $k_w = 0$, stress and porosity evolutions coincide with the original GTN model. The results show that the modified GTN model can predict damage accumulation in shear stress conditions.

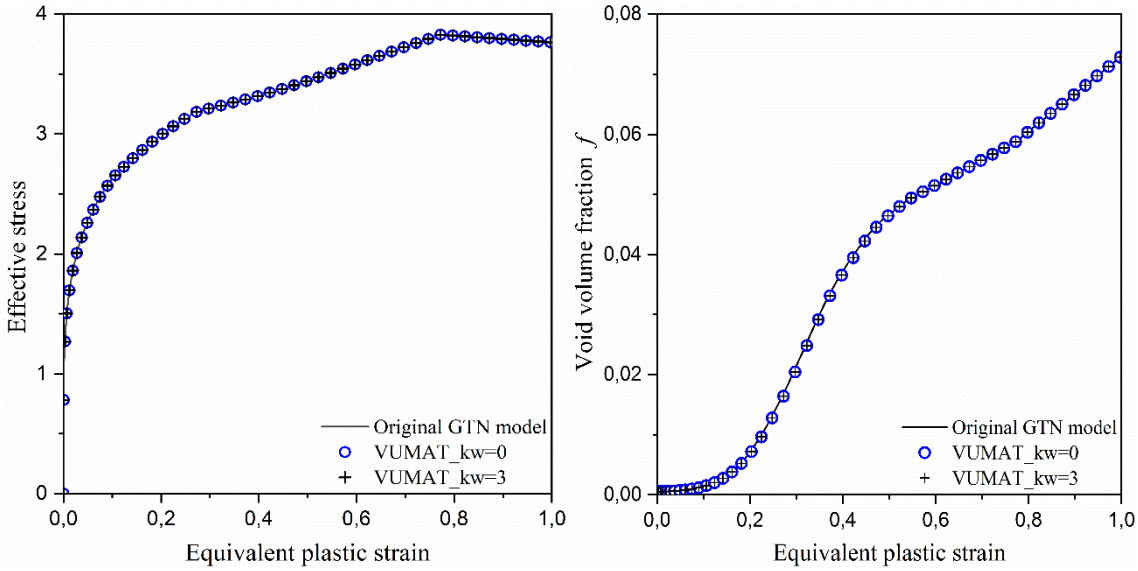

(a) **(b)**

Fig. 2. Uniaxial tension test as a function of the equivalent plastic strain: (a) Effective stress (b) void volume fraction.

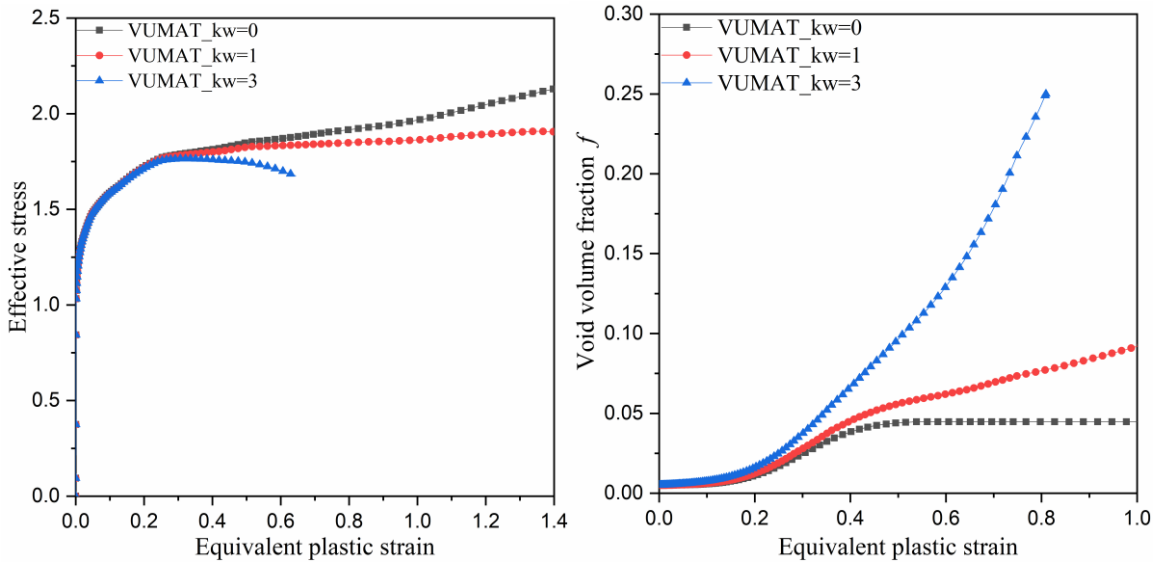

(a) **(b)**

Fig. 3. Simple shear test as a function of the equivalent plastic strain for k_w = 0, 1, 3: (a) Effective stress (b) void volume fraction.

3. Material and methods

In this section, the material used for this study is presented and the considered mechanical behavior law is introduced. Several tensile tension and micro incremental sheet forming tests are then performed experimentally and equivalent numerical models are developed to calibrate the constitutive parameters of the modified GTN model by an inverse method.

3.1. Material parameter and hardening law

The selected material is a 210 µm thick sheet in a Cu-0.1Fe copper alloy. The material is annealed at 400°C for 30 minutes to eliminate the effects of rolling texture and to homogenize the material microstructure [43].

Uniaxial tensile tests are conducted according to the ISO 3167 standard. The use of this standard is justified by the very thin thickness (210 µm) of the sheet used in this study, made of copper alloy. The tests are performed on flat specimens in three directions 0°, 45°, and 90° with respect to the rolling direction (figure 4). The measurements of the elongation Δl were performed using a laser extensometer. Three tests are conducted for each direction to minimize experimental deviation. The specimen is elongated up to fracture, and the true stress-strain curves are presented in Figure 5.

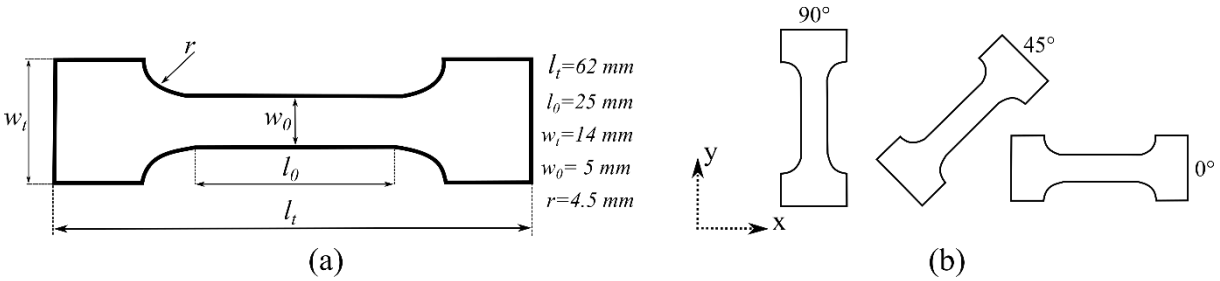

Fig. 4. Tensile test specimen (a) Geometry and characteristic dimensions (in mm), (b) direction tests.

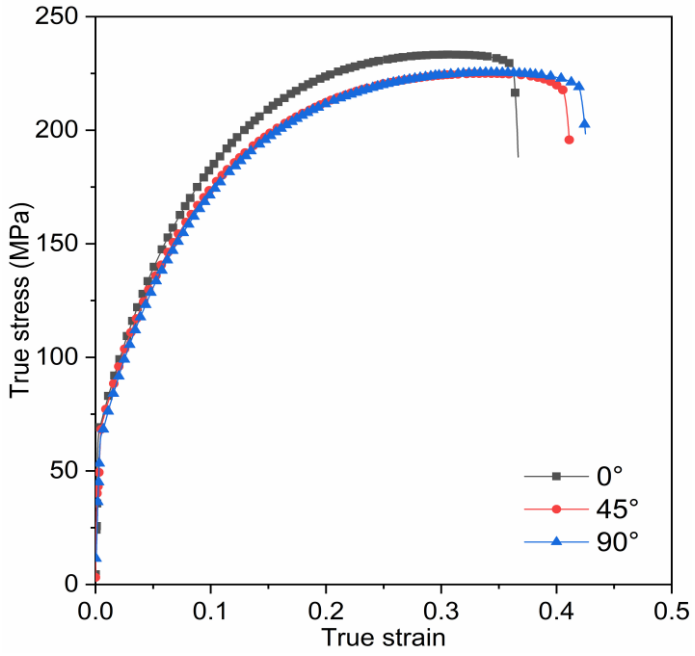

Fig. 5. True stress-true strain curves.

The stress-strain curves presented in Figure 5 illustrate small deviations. Lankford's coefficients (r_0, r_{45} and r_{90}) are measured up to 20% of strain. The calculated normal anisotropy and the planar anisotropy are $R_N = 0.9874$ and $\Delta R = -0.12$, respectively. These results demonstrate that the material can be considered isotropic. The elastic parameters obtained from ultrasonic characterization are 100 GPa for the Young Modulus and 0.31 for the Poisson's ratio. These results are in good agreement with data reported in the literature [44, 45].

The Voce's isotropic hardening behavior of the matrix is considered [46] and can be described by

$$\bar{\sigma} = \sigma_y + Q(1 - exp(-b\bar{\varepsilon}^p)) \quad (10)$$

where $\bar{\sigma}$ is the equivalent stress, $\bar{\varepsilon}^p$ is the equivalent plastic strain, σ_y is the initial yielding stress, Q and b are isotropic hardening parameters.

To provide an accurate prediction of the material behavior, the shear-modified GTN model described in section 2 is used for the numerical modeling. Therefore, the set of 10 parameters $q_1, q_2, q_3, f_0, f_N, \varepsilon_N, S_N, f_c, f_F$ and k_w, have to be identified.

These parameters are divided into categories associated with the contribution of elasticity, plasticity, and damage. In order to minimize the number of damage parameters to calibrate, some of them can be set as constants according to the literature [7, 17, 47]. The combination $q_1 = 1.5,\ q_2 = 1.0,\ q_3 = q_1^2$ is selected and fits most metal materials [25]. Also: ε_N and S_N are constant and can be fixed to 0.3 and 0.1 respectively [48]. Finally, for the identification of: f_0, f_N, f_c, f_F and k_w, a finite element inverse method is proposed.

3.2. Calibration methods of the GTN model parameters

The identification of the modified GTN model parameters is performed from a micro-SPIF test using the finite element updating method (FEUM). For this, a comparison between numerical simulations and experimental results of the forming forces along the forming axis is used as presented by Hapsari et al. [38]. The finite element inverse method based on the minimization of a function of cost is employed for the identification. The Levenberg-Marquardt optimization algorithm [49, 50] is used through the **MIC2M** software identification toolkit developed on MATLAB by Richard [51] for the parameters identification.

As described in Figure 6, the procedure of identification is adapted to the identification of the proposed model and divided into 2 steps. The first step is dedicated to the identification of elastic and initial plastic parameters using tensile test results to obtain a physical solution and reduce computing time. The second one uses the results of step 1 as input data for the identification of plastic and the modified GTN damage model parameters by comparing forming forces between the experimental µ-SPIF test and modeling.

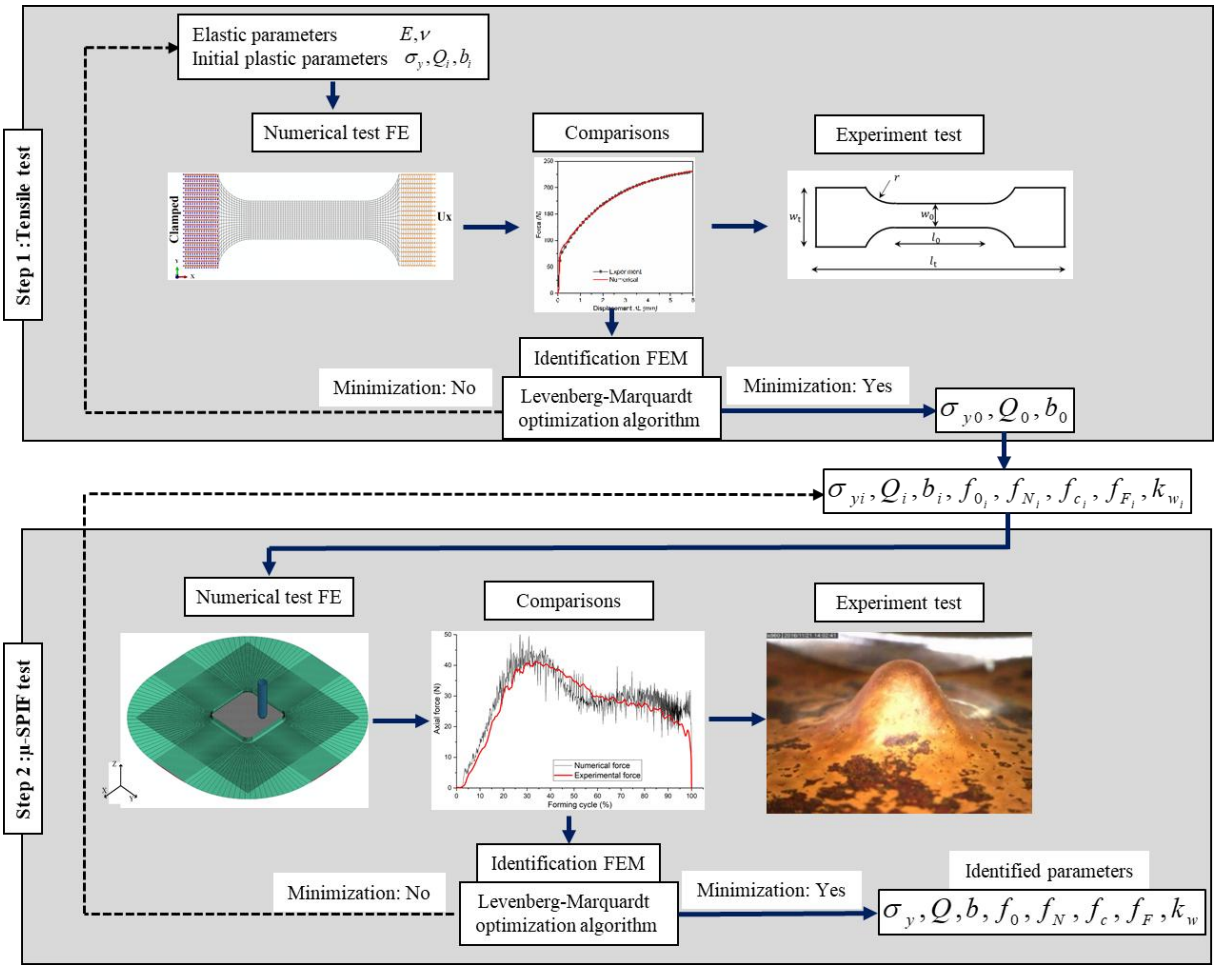

Fig. 6. Identification procedure of GTN model parameters.

3.2.1. Identification with tensile test (Step #1)

The first step is devoted to the calibration of the elastic parameters and the initial hardening set parameters using a tensile test. The identification approach is applied to the tensile force by comparing numerical and experimental data.

For the experimental part, uniaxial tensile tests are performed as previously described in section.3.1. A finite element simulation of the tensile tests is carried out with the same experimental conditions. Using ABAQUS/Explicit software, the specimen is meshed by 4-node quadrilateral shell elements (S4R) to decrease the computational time. For boundary conditions, the specimen is fixed on the left while, on the right side a displacement is applied in the x-direction, as illustrated in figure 7. The Force evolution is obtained by summing the nodal forces at the fixed end of the specimen.

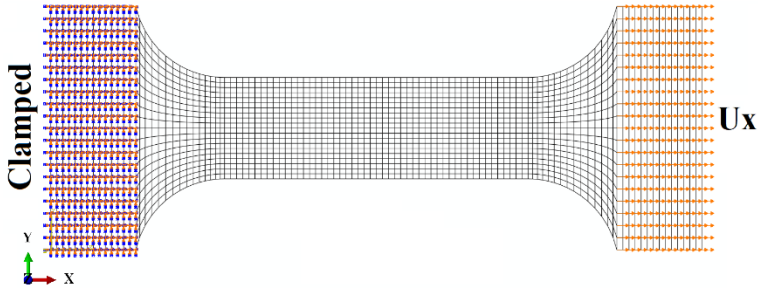

Fig. 7. Finite element model used for tensile tests.

The initial hardening parameters (σ_{y0}, Q_0, b_0) from the tensile test are obtained using the FEUM method. For each simulation, a comparison of the numerical reaction force to the experimental measurement is done and the initial hardening parameters are iteratively adjusted until the cost function is minimized using the Levenberg-Marquardt optimization algorithm. The identification of the considered parameters is made until 25% of deformation to avoid the influence of the necking phenomenon.

3.2.2. Identification using µ-SPIF test (Step #2)

The second step is dedicated to the identification of the remaining model parameters based on the results of step #1 and with modeling and experimental µ-SPIF tests combination.

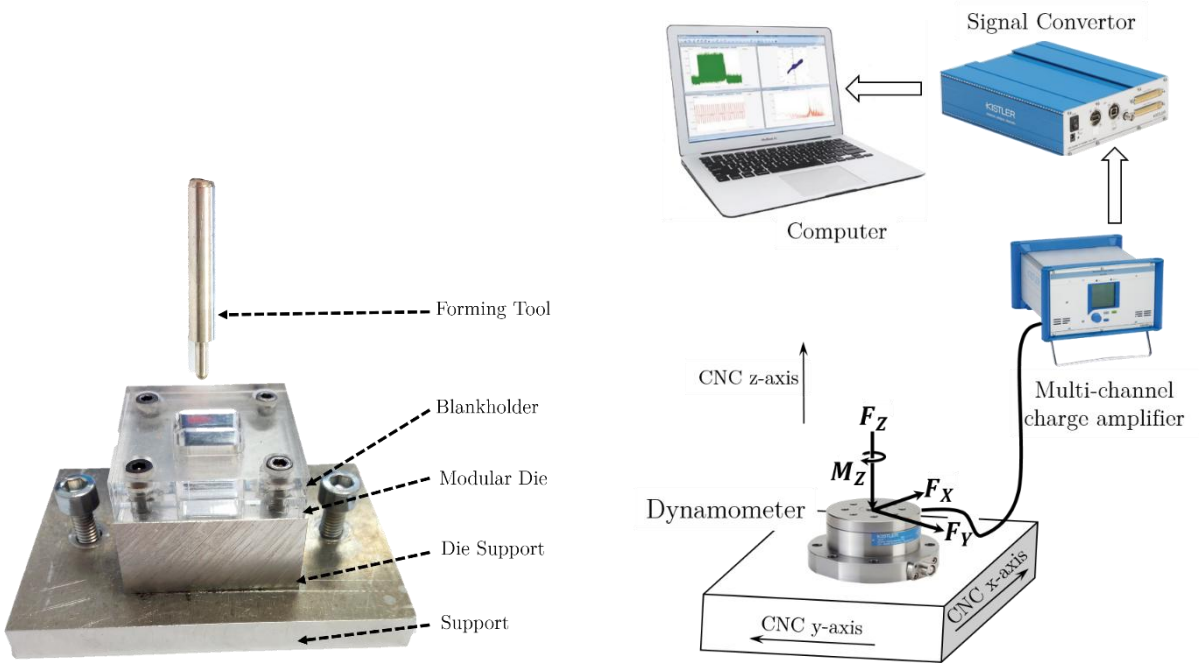

(a) **(b)**

Fig. 8. Micro-SPIF test: (a) testing device, (b) forces acquisition.

An experimental device used as a platform for the µ-SPIF tests is mounted on a CNC milling machine (figure 8a). The forming forces F_z are acquired by using a 4-axis dynamometer, as represented in Figure 8b. The dynamometer is mounted between a testing device and the machine work-surface and connected to a multi-channel charge amplifier. The measuring system also includes data acquisition cards and a computer. In order to reduce friction between the tool and the workpiece, water/oil mixture fluid, composed of 5% cutting oil and 95% water, is used as a lubricant to improve the sheet's formability. Each test is repeated three times to ensure the reliability of the tests. Pyramidal shape is used to perform the µ-SPIF test with a helical forming strategy. The geometrical definition and strategy are presented in Figure 9. The main µ-SPIF process parameters are given in Table .1.

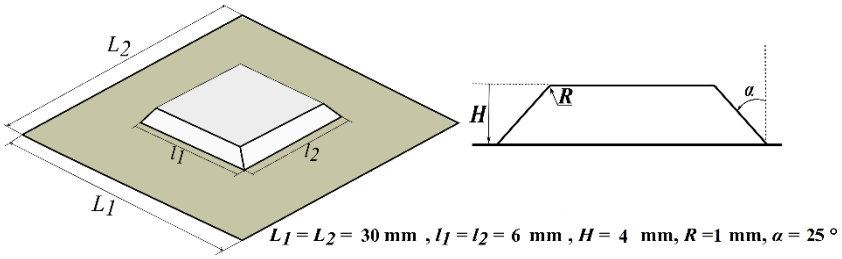

(a)

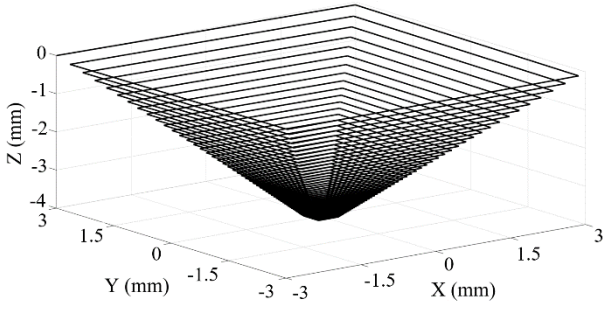

(b)

Fig. 9. (a) Pyramidal geometry, (b) helical forming strategies.

Table 1
SPIF process parameters and geometry

Tool diameter	1.9 mm
Tool depth step	0.1 mm
Spindle speed	1000 rpm
Feed rate	300 mm/min

For the numerical model, a fully parametric toolbox, programmed and developed in the study of Thibaud et al. [52], is adapted for the simulation of the µ-SPIF test under the commercial finite element code Abaqus/Explicit. This parametric toolbox also defines the experimental path in CNC language machine by way of parametric paths to perform experiments and simulations with the same trajectories. A parametric model (mesh, boundary, loading, initial conditions, material behavior) is first produced and then used as the input files to run the simulations of µ-SPIF.

The simulation conditions (geometry, boundary, load, and initial conditions) of the µ-SPIF are the same as those used for the study of the forming of the pyramid shape. The blank is meshed with fully integrated 8-node solid elements (C3D8). To get information on the thickness evolution, three elements in thickness are considered. The rest of the tooling (forming tool, die, and blank holder) has meshed with rigid shell elements (R3D4). Coulomb frictional

contact behavior is used at the interfaces between the forming tool and the metal sheet, with a friction coefficient value of 0.2 [52]. The finite element model is illustrated in Figure 10.

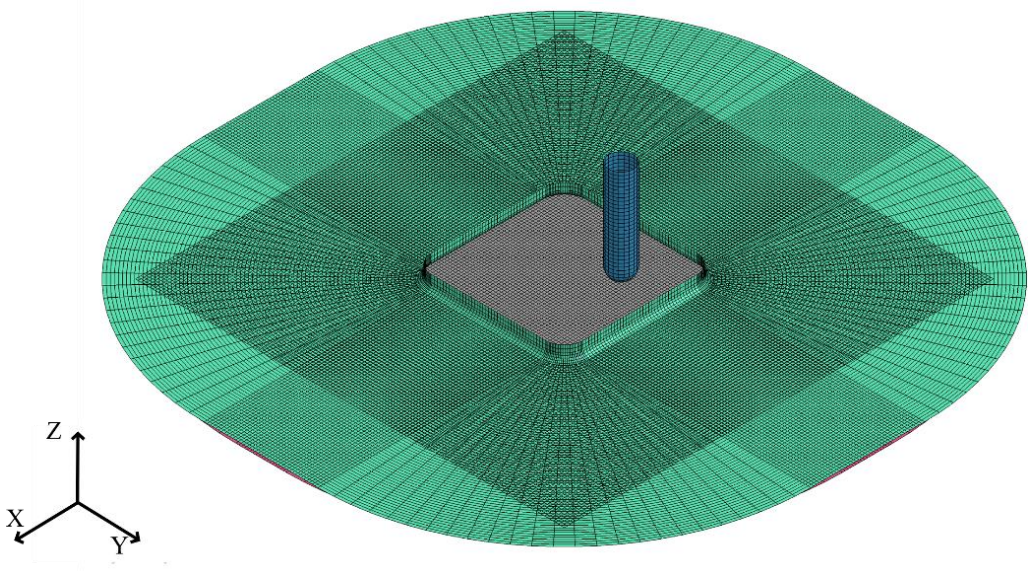

Fig. 10. Mesh model of µ-SPIF simulations.

The identified elastic-plastic parameters (σ_{y0}, Q_0, b_0) obtained from step #1 (physical solution) are introduced as the initial values for the second step.

The initial values of damage parameters are taken from the literature [30, 31]. The numerical results (forming force) of µ-SPIF are compared to the experimental measurements. Then, the same iterative optimization algorithm used in step #1 is applied to adjust the material parameters on smooth forming force evolutions.

4. Results and discussion

4.1. Tensile test (Step #1)

The calibration via a tensile test of the plastic parameters (σ_{y0}, Q_0, b_0) took 8 hours of simulation with 11 iterations of the inverse method. Parallel processing is utilized with 16 processors for reducing the simulation time. The obtained results are presented in Table .2. The comparison between the hardening model response and the experimental load-displacement curve is given in Figure 11. The model with the identified plastic parameters is close to the experimental curve.

Table 2
Material parameters calibrated from tensile test

$\sigma_{y0}\,(MPa)$	$Q_0\,(MPa)$	b_0
65.87	172.57	30.1

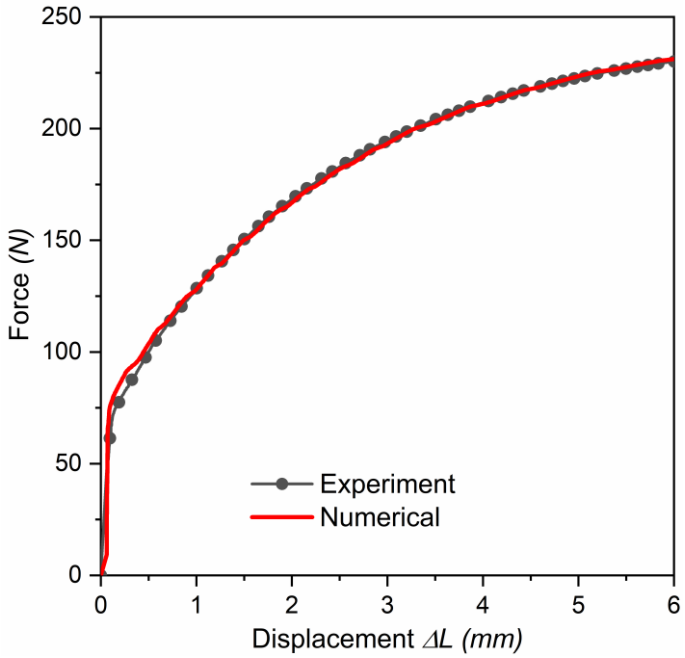

Fig. 11. Experimental and model comparisons of force-displacement tensile curves.

4.2. Micro-SPIF test (Step #2)

Due to the important size of the problem and the stability condition associated with the explicit algorithm, simulation time requires approximately 15 hours for each iteration of µ-SPIF simulation. Therefore, parallel calculation of Abaqus/Explicit is used with 8 processors to decrease the computational time. The results are then obtained after 15 iterations corresponding to a total computation time of 225 hours. The obtained set of calibration parameters is reported in Table .3. The comparison between the numerical and the experimental axial forces F_z of the process as a function of the forming cycle is shown in Figure 12.

Table 3
Material parameters calibrated by using the Micro-SPIF test

$\sigma_{y0}\,(MPa)$	$Q_0\,(MPa)$	b_0	f_0	f_N	f_c	f_F	k_w
65.87	177.4	30.34	1.23E-3	4.08E-3	2.49E-3	0.13	0.86

The experimental axial forming force is correctly reproduced by numerical modeling. A difference at the beginning, at 20% of the forming cycle, could be due to the initial contact between the forming tool and the blank. The tool is considered rigid and stable during forming, but this assumption is not valid for elastic contact, which will affect the evolution of the forming force at the beginning of the cycle. When a local plastic strain occurs, the evolution of the numerical process becomes close to the experimental data for the rest of the forming cycle.

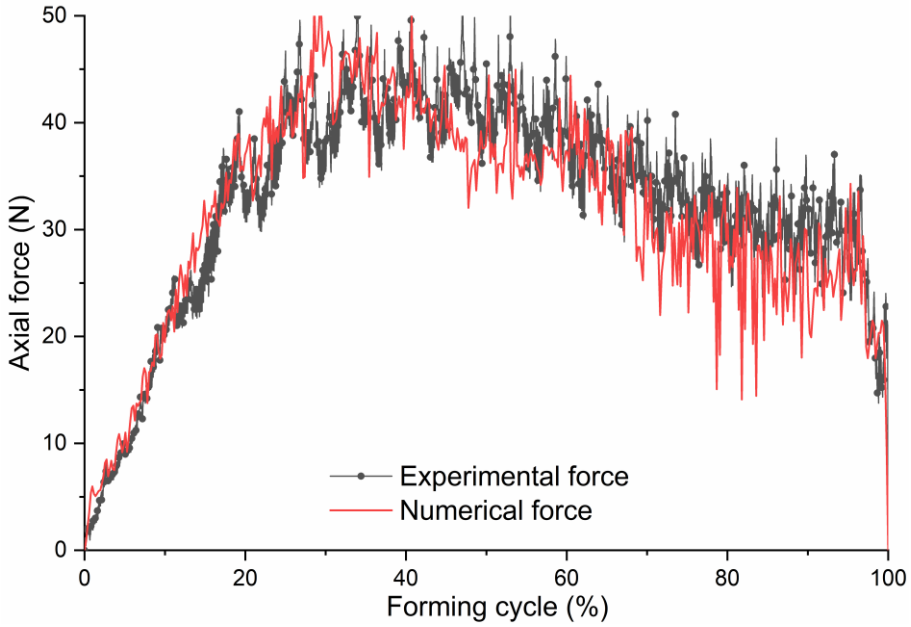

Fig. 12. Evolutions of numerical and experimental axial forming forces using the helical strategy and pyramidal geometry after the identification procedure.

A general geometric comparison between the experimental profile obtained by an ALICONA Infinite Focus Microscope and the numerical one is carried out to improve the quality of the parts obtained by the µ-SPIF process (figure 13). The pyramidal shape obtained by numerical simulation is close to the experimental part. The differences observed can be explained by the reasons of the low thickness of the sheet and the effect of springback, which is a difficult parameter to control.

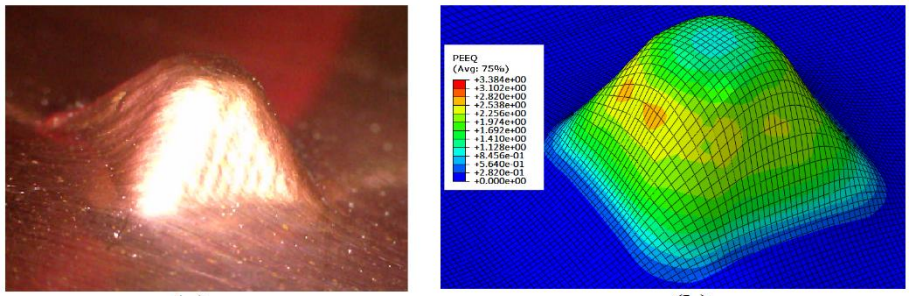

(a) **(b)**

Fig. 13. Evolutions of numerical and experimental axial forming forces using the helical strategy and pyramidal geometry.

4.3. Validation tests

In this section, the validation of the identified behavior law is studied. The calibrated material parameters identified in the previous section are used to simulate the validation tests. For this, a series of experimental µ-SPIF tests are carried out and compared with the numerical results using the identified damage parameters. A pyramidal shape with a constant Z-level strategy and a conical-shaped part using both forming strategies (constant Z-level and helical) is adopted. The obtained results of forming forces and geometric accuracy are compared to the experimental data and given in the figure. 14.

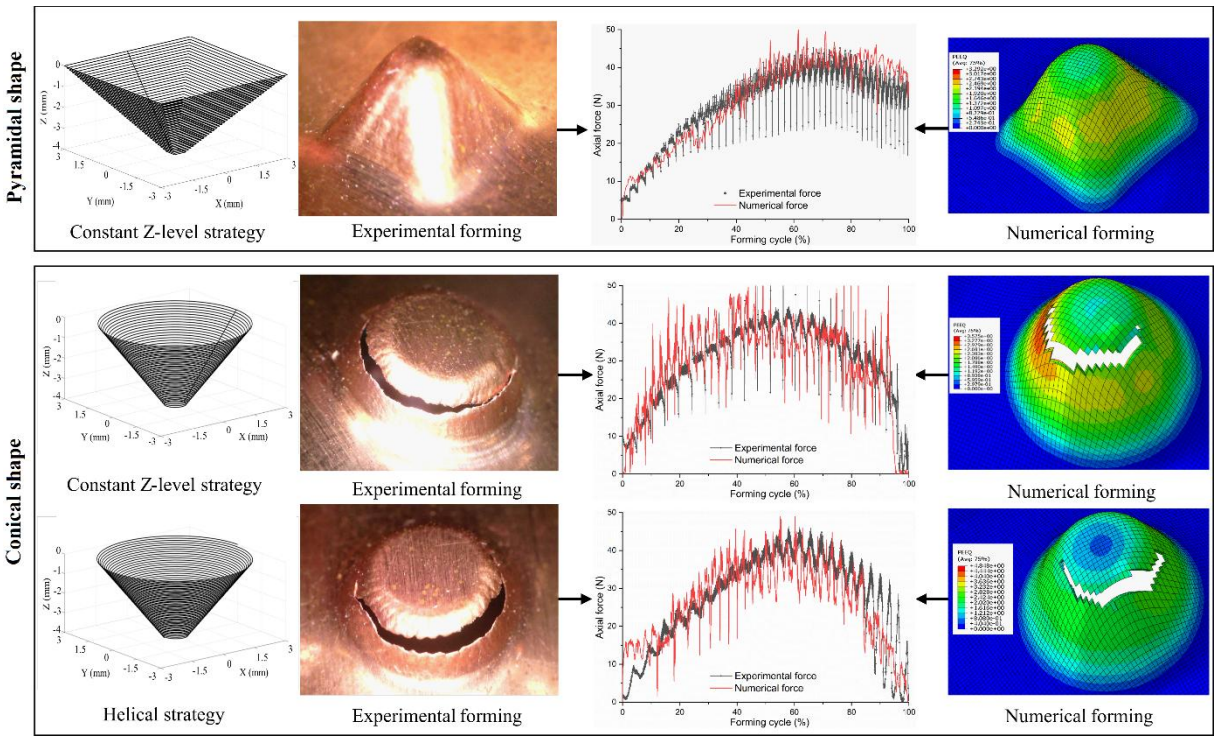

Fig. 14. Validation approach of the ductile damage model.

The simulation of the pyramidal shape with constant Z-level strategy shows a good correspondence with the real part for the overall geometry, as presented in Figure 14. The results obtained show that the evolution of the numerical forming force is also close to the experimental measurement. A small difference is observed at the beginning of the forming cycle (10%) and disruption in the numerical effort due to the nature of the Z-constant trajectory, which generates tool/part contact discontinuity. These observations show that the strain paths are not the same between the two strategies. For the conical shapes. A good agreement is obtained between the numerically predicted forming force and that measured experimentally in terms of forming force level and geometric accuracy.

However, a discrepancy in the prediction of the moment of failure during the simulation of the conical shape is observed. This discrepancy can be attributed to the choice of material parameters. Indeed, the identification procedure was tested and verified using the pyramid shape (which showed good results in predicting the evolution of the force and the final shape during failure). Therefore, the differences observed in the simulation of the conical shapes could be reduced by introducing an identifiability analysis in the identification method which makes it possible to control the capacity to effectively identify the parameters of the model [53, 54].

Crack is observed from the significant decrease in the force level to zero, which corresponds to about 95% of the forming cycle for both forming strategies. The force level differences (alternation between a zero and a positive value) at the end of the forming cycle are due to the

alternative contact between the tool and the sheet (displacement with the cracked top of the part).

5. Conclusions

The paper is dedicated to the identification of the ductile damage behavior of thin sheet metals via micro-single point incremental forming tests. A micromechanical GTN model modified for shear loading is chosen for the prediction of the damage and ductile fracture of materials applied to a single-phase copper alloy. This model is implemented as a user material constitutive subroutine in ABAQUS/Explicit. A parametric finite elements model procedure based on the inverse method is developed and coupled with experimental tests to calibrate the shear-modified GTN damage model parameters. The identification of the considered parameters is carried out by the minimization of the gap between the forming forces in the µ-SPIF test and modeling. This approach is divided into two principles steps:

- The first step is dedicated to the identification of elastic and initial plastic parameters using tensile tests at moderate plastic strain level (25%).
- The second step uses the results of step #1 as input data for the identification of plastic and the modified GTN damage model parameters under large local strains level (>150%).

The validity of the identified material damage parameters is confirmed by comparing the simulations of several incremental forming tests to experimental results. The obtained results of the validation tests showed good agreement compared with the experimental measurements. Therefore, the identified damage parameters of the shear-modified GTN damage model are effective to characterize the damage evolution and ductile failure in the ISF process.

Future studies will focus on improving the identification method by introducing an identifiability analysis that allows controlling the ability to identify model parameters efficiently. Once the identification of the parameters has been carried out, simulations of incremental forming could be carried out to optimize the process, in particular the toolpath that minimizes the geometric differences between the designed part and the manufactured one. In order to improve the prediction of when and where the material damage occurs when studying the microforming of thin structures, we plan to use a physically based model taking into account the shape change and the rotation of the cavities [55–57]. Indeed, microforming processes such as the one presented in this study are accompanied by a consistent rotation of the material, it is, therefore, necessary to include coherently its effect on the damage of the material.

Compliance with Ethical Standards

Conflict of interest Authors declare that they do not have any commercial or associative interest that represents a conflict of interest in connection with the work submitted.

Funding The authors declare that no funds, grants, or other support were received during the preparation of this manuscript.

References

1. Duflou, J. R., Habraken, A.-M., Cao, J., Malhotra, R., Bambach, M., Adams, D., … Jeswiet, J. (2018). Single point incremental forming: state-of-the-art and prospects. International Journal of Material Forming, 11(6), 743–773. https://doi.org/10.1007/s12289-017-1387-y
2. McClintock, F. A. (1968). A Criterion for Ductile Fracture by the Growth of Holes. Journal of Applied Mechanics, 35(2), 363–371. https://doi.org/10.1115/1.3601204
3. Rice, J. R., & Tracey, D. M. (1969). On the ductile enlargement of voids in triaxial stress fields∗. Journal of the Mechanics and Physics of Solids, 17(3), 201–217. https://doi.org/10.1016/0022-5096(69)90033-7
4. Gurson, A. L. (1977). Continuum Theory of Ductile Rupture by Void Nucleation and Growth: Part I—Yield Criteria and Flow Rules for Porous Ductile Media. Journal of Engineering Materials and Technology, 99(1), 2–15. https://doi.org/10.1115/1.3443401
5. Tvergaard, V. (1981). Influence of voids on shear band instabilities under plane strain conditions. International Journal of Fracture, 17(4), 389–407. https://doi.org/10.1007/BF00036191
6. Tvergaard, V. (1982). Influence of void nucleation on ductile shear fracture at a free surface. Journal of the Mechanics and Physics of Solids, 30(6), 399–425. https://doi.org/10.1016/0022-5096(82)90025-4
7. Tvergaard, V., & Needleman, A. (1984). Analysis of the cup-cone fracture in a round tensile bar. Acta Metallurgica, 32(1), 157–169. https://doi.org/10.1016/0001-6160(84)90213-X
8. Besson, J., Devillers-Guerville, L., & Pineau, A. (2000). Modeling of scatter and size effect in ductile fracture: application to thermal embrittlement of duplex stainless steels. Engineering Fracture Mechanics, 67(2), 169–190. https://doi.org/10.1016/S0013-7944(00)00056-4
9. Chen, Z., & Dong, X. (2009). The GTN damage model based on Hill'48 anisotropic yield criterion and its application in sheet metal forming. Computational Materials Science, 44(3), 1013–1021. https://doi.org/10.1016/j.commatsci.2008.07.020
10. Kiran, R., & Khandelwal, K. (2014). Gurson model parameters for ductile fracture simulation in ASTM A992 steels: gurson model parameters for ductile fracture simulation in astm a992 steels. Fatigue & Fracture of Engineering Materials & Structures, 37(2), 171–183. https://doi.org/10.1111/ffe.12097
11. Benzerga, A. A., Leblond, J.-B., Needleman, A., & Tvergaard, V. (2016). Ductile failure modeling. International Journal of Fracture, 201(1), 29–80. https://doi.org/10.1007/s10704-016-0142-6
12. Aldakheel, F., Wriggers, P., & Miehe, C. (2018). A modified Gurson-type plasticity model at finite strains: formulation, numerical analysis and phase-field coupling. Computational Mechanics, 62(4), 815–833. https://doi.org/10.1007/s00466-017-1530-0

13. Ould Ouali, M. (2018). Relevance of Incorporating Cavity Shape Change in Modelling the Ductile Failure of Metals. Mathematical Problems in Engineering, 2018, 1–9. https://doi.org/10.1155/2018/6454790

14. He, Z., Zhu, H., & Hu, Y. (2021). An improved shear modified GTN model for ductile fracture of aluminium alloys under different stress states and its parameters identification. International Journal of Mechanical Sciences, 192, 106081. https://doi.org/10.1016/j.ijmecsci.2020.106081

15. Bao, Y., & Wierzbicki, T. (2004). On fracture locus in the equivalent strain and stress triaxiality space. International Journal of Mechanical Sciences, 46(1), 81–98. https://doi.org/10.1016/j.ijmecsci.2004.02.006

16. Lou, Y., & Huh, H. (2013). Evaluation of ductile fracture criteria in a general three-dimensional stress state considering the stress triaxiality and the lode parameter. Acta Mechanica Solida Sinica, 26(6), 642–658. https://doi.org/10.1016/S0894-9166(14)60008-2

17. Xue, L. (2008). Constitutive modeling of void shearing effect in ductile fracture of porous materials. Engineering Fracture Mechanics, 75(11), 3343–3366. https://doi.org/10.1016/j.engfracmech.2007.07.022

18. Nahshon, K., & Hutchinson, J. W. (2008). Modification of the Gurson Model for shear failure. European Journal of Mechanics - A/Solids, 27(1), 1–17. https://doi.org/10.1016/j.euromechsol.2007.08.002

19. Malcher, L., Reis, F. J. P., Andrade Pires, F. M., & César de Sá, J. M. A. (2013). Evaluation of shear mechanisms and influence of the calibration point on the numerical results of the GTN model. International Journal of Mechanical Sciences, 75, 407–422. https://doi.org/10.1016/j.ijmecsci.2013.08.008

20. Malcher, L., Andrade Pires, F. M., & César de Sá, J. M. A. (2014). An extended GTN model for ductile fracture under high and low stress triaxiality. International Journal of Plasticity, 54, 193–228. https://doi.org/10.1016/j.ijplas.2013.08.015

21. Kami, A., Dariani, B., sadough vanini, S. ali, Comsa, D.-S., & Banabic, D. (2014). Application of a GTN Damage Model to Predict the Fracture of Metallic Sheets Subjected to Deep-Drawing. Proceedings of the Romanian Academy - Series A: Mathematics, Physics, Technical Sciences, Information Science, 15, 300–309.

22. Kami, A., Dariani, B. M., Sadough Vanini, A., Comsa, D. S., & Banabic, D. (2015). Numerical determination of the forming limit curves of anisotropic sheet metals using GTN damage model. Journal of Materials Processing Technology, 216, 472–483. https://doi.org/10.1016/j.jmatprotec.2014.10.017

23. Gatea, S., Ou, H., Lu, B., & McCartney, G. (2017). Modelling of ductile fracture in single point incremental forming using a modified GTN model. Engineering Fracture Mechanics, 186, 59–79. https://doi.org/10.1016/j.engfracmech.2017.09.021

24. belouettar, K., Mohand, O. O., Nasereddine, Z., & Sébastien, T. (2021). Investigation of the influence of incremental sheet forming process parameters using response surface methodology. Metallurgical Research & Technology, 118(4), 401. https://doi.org/10.1051/metal/2021039

25. Ying, L., Wang, D., Liu, W., Wu, Y., & Hu, P. (2018). On the numerical implementation of a shear modified GTN damage model and its application to small punch test. International Journal of Material Forming, 11(4), 527–539. https://doi.org/10.1007/s12289-017-1362-7

26. Achouri, M., Germain, G., Dal Santo, P., & Saidane, D. (2013). Numerical integration of an advanced Gurson model for shear loading: Application to the blanking process.

Computational Materials Science, 72, 62–67. https://doi.org/10.1016/j.commatsci.2013.01.035

27. Achouri, M., Germain, G., Dal Santo, P., & Saidane, D. (2013). Experimental characterization and numerical modeling of micromechanical damage under different stress states. Materials & Design, 50, 207–222. https://doi.org/10.1016/j.matdes.2013.02.075

28. Aguir, H., & Marouani, H. (2010). Gurson-Tvergaard-Needleman parameters identification using artificial neural networks in sheet metal blanking. International Journal of Material Forming, 3(S1), 113–116. https://doi.org/10.1007/s12289-010-0720-5

29. Marouani, H., & Aguir, H. (2012). Identification of material parameters of the Gurson–Tvergaard–Needleman damage law by combined experimental, numerical sheet metal blanking techniques and artificial neural networks approach. International Journal of Material Forming, 5(2), 147–155. https://doi.org/10.1007/s12289-011-1035-x

30. Abbassi, F., Belhadj, T., Mistou, S., & Zghal, A. (2013). Parameter identification of a mechanical ductile damage using Artificial Neural Networks in sheet metal forming. Materials & Design, 45, 605–615. https://doi.org/10.1016/j.matdes.2012.09.032

31. Sun, Q., Lu, Y., & Chen, J. (2020). Identification of material parameters of a shear modified GTN damage model by small punch test. International Journal of Fracture, 222(1–2), 25–35. https://doi.org/10.1007/s10704-020-00428-4

32. Corigliano, A., Mariani, S., & Orsatti, B. (2000). Identification of Gurson–Tvergaard material model parameters via Kalman filtering technique. I. Theory. International Journal of Fracture, 104(4), 349–373. https://doi.org/10.1023/A:1007602106711

33. Springmann, M., & Kuna, M. (2005). Identification of material parameters of the Gurson–Tvergaard–Needleman model by combined experimental and numerical techniques. Computational Materials Science, 32(3–4), 544–552. https://doi.org/10.1016/j.commatsci.2004.09.010

34. Springmann, M., & Kuna, M. (2006). Determination of Ductile Damage Parameters by Local Deformation Fields: Measurement and Simulation. Archive of Applied Mechanics, 75(10–12), 775–797. https://doi.org/10.1007/s00419-006-0033-9

35. Muñoz-Rojas, P. A., Cardoso, E. L., & Vaz, M. (2010). Parameter Identification of Damage Models Using Genetic Algorithms. Experimental Mechanics, 50(5), 627–634. https://doi.org/10.1007/s11340-009-9321-y

36. Ghouati, O., & Gelin, J. C. (1998). Identification of material parameters directly from metal forming processes. Journal of Materials Processing Technology, 80–81, 560–564. https://doi.org/10.1016/S0924-0136(98)00159-9

37. Ben Hmida, R., Richard, F., Thibaud, S., & Malécot, P. (2015). Elastic-Plastic Damage Behavior Identification in Micro Scale Length from Instrumented Micro-Single Point Incremental Forming (pp. 230–233). Research Publishing Services. https://doi.org/10.3850/978-981-09-4609-8_059

38. Hapsari, G., Richard, F., Ben Hmida, R., Malécot, P., & Thibaud, S. (2018). Instrumented Incremental Sheet Testing for material behavior extraction under very large strain: Information richness of continuous force measurement. Materials & Design, 140, 317–331. https://doi.org/10.1016/j.matdes.2017.12.002

39. Aravas, N. (1987). On the numerical integration of a class of pressure-dependent plasticity models. International Journal for Numerical Methods in Engineering, 24(7), 1395–1416. https://doi.org/10.1002/nme.1620240713

40. Zhang, Z. L. (1995). Explicit consistent tangent moduli with a return mapping algorithm for pressure-dependent elastoplasticity models. Computer Methods in Applied Mechanics and Engineering, 121(1–4), 29–44. https://doi.org/10.1016/0045-7825(94)00707-T

41. Ben Chabane, N., Aguechari, N., & Ould Ouali, M. (2022). Study of the slant fracture in solid and hollow cylinders: Experimental analysis and numerical prediction. Frattura ed Integrità Strutturale, 17(63), 169–189. https://doi.org/10.3221/IGF-ESIS.63.15

42. Nahshon, K., & Xue, Z. (2009). A modified Gurson model and its application to punch-out experiments. Engineering Fracture Mechanics, 76(8), 997–1009. https://doi.org/10.1016/j.engfracmech.2009.01.003

43. Ben Hmida, R., Thibaud, S., Gilbin, A., & Richard, F. (2013). Influence of the initial grain size in single point incremental forming process for thin sheets metal and microparts: Experimental investigations. Materials & Design, 45, 155–165. https://doi.org/10.1016/j.matdes.2012.08.077

44. Gréban, F., Monteil, G., & Roizard, X. (2007). Influence of the structure of blanked materials upon the blanking quality of copper alloys. Journal of Materials Processing Technology, 186(1–3), 27–32. https://doi.org/10.1016/j.jmatprotec.2006.11.226

45. Hapsari, G., Thibaud, S., Richard, F., Malécot, P., Hmida, R. B., & Bonnardot, C. (2020). Thin Sheet Behaviour Identification by µ-InDef and Identifiability Analysis. Procedia Manufacturing, 47, 1481–1489. https://doi.org/10.1016/j.promfg.2020.04.330

46. Voce, E. (1955). A practical strain-hardening function. Metallurgica, 51, 219–226.

47. Oh, C.-K., Kim, Y.-J., Baek, J.-H., Kim, Y.-P., & Kim, W. (2007). A phenomenological model of ductile fracture for API X65 steel. International Journal of Mechanical Sciences, 49(12), 1399–1412. https://doi.org/10.1016/j.ijmecsci.2007.03.008

48. Nielsen, K. L., & Tvergaard, V. (2009). Effect of a shear modified Gurson model on damage development in a FSW tensile specimen. International Journal of Solids and Structures, 46(3–4), 587–601. https://doi.org/10.1016/j.ijsolstr.2008.09.011

49. Levenberg, K. (1944). A method for the solution of certain non-linear problems in least squares. Quarterly of Applied Mathematics, 2(2), 164–168.

50. Marquardt, D. W. (1963). An Algorithm for Least-Squares Estimation of Nonlinear Parameters. Journal of the Society for Industrial and Applied Mathematics, 11(2), 431–441.

51. Richard, F. (1999). MIC2M: Modélisation et Identification du Comportement Mécanique des Matériaux. Université de Franche-Comté. Retrieved from http://mic2m.univ-fcomte.fr

52. Thibaud, S., Ben Hmida, R., Richard, F., & Malécot, P. (2012). A fully parametric toolbox for the simulation of single point incremental sheet forming process: Numerical feasibility and experimental validation. Simulation Modelling Practice and Theory, 29, 32–43. https://doi.org/10.1016/j.simpat.2012.07.004

53. Brun, R., Reichert, P., & Künsch, H. R. (2001). Practical identifiability analysis of large environmental simulation models. Water Resources Research, 37(4), 1015–1030. https://doi.org/10.1029/2000WR900350

54. Richard, F., Villars, M., & Thibaud, S. (2013). Viscoelastic modeling and quantitative experimental characterization of normal and osteoarthritic human articular cartilage using indentation. Journal of the Mechanical Behavior of Biomedical Materials, 24, 41–52. https://doi.org/10.1016/j.jmbbm.2013.04.012

55. Ould Ouali, M., & Aberkane, M. (2009). Micromechanical modeling of the rolling of a A1050P aluminum sheet. International Journal of Material Forming, 2(1), 25–36. https://doi.org/10.1007/s12289-008-0387-3

56. Torki, M. E., Tekoğlu, C., Leblond, J.-B., & Benzerga, A. A. (2017). Theoretical and numerical analysis of void coalescence in porous ductile solids under arbitrary loadings. International Journal of Plasticity, 91, 160–181. https://doi.org/10.1016/j.ijplas.2017.02.011

57. Khan, I. A., Srivastava, A., Needleman, A., & Benzerga, A. A. (2021). An analysis of deformation and failure in rectangular tensile bars accounting for void shape changes. International Journal of Fracture, 230(1–2), 133–156. https://doi.org/10.1007/s10704-021-00532-z